Acta Crystallographica Section B
Structural Science
ISSN 0108-7681

Crystallographic input data for (001)-, (110)- and (111)-oriented superlattices

Z Touaa[a] and Nadir Sekkal[b,c,d]*

[a]Département de Physique-Chimie, Ecole Normale Supérieure de l'Enseignement Technologique, BP 1523 EL M'Naouer, Oran 31000, Algeria, [b]Laboratoire de Caractérisation et Simulation des Composants et Circuits électroniques (CaSiCCe), ENSET-Oran, BP 1523 EL M'Naouer, Oran 31000, Algeria, [c]Laboratoire de Microphysique et de Nanophysique (LaMiN), ENSET-Oran, BP 1523 EL M'Naouer, Oran 31000, Algeria, and [d]Physia-Laboratory, BP 47 (RP), Sidi Bel Abbès 22000, Algeria

Correspondence e-mail: nsekkal@yahoo.fr

Received 10 May 2012
Accepted 2 July 2012

General aspects concerned with (001)-, (110)- and (111)-oriented superlattices (SLs) have been investigated. In particular, the symmetry of these systems have been derived and given in detail. As a test, the obtained data have been utilized to calculate electronic structures and gaps of a standard GaAs/AlAs system using an accurate version of the first principle full potential linear muffin-tin orbital (FPLMTO) method based on a local-density functional approximation (LDA).

1. Introduction

It is well known that the crystal orientations have a significant impact on their properties and their potential applications. They can be generated artificially during the growth process but they can also occur naturally since a change of orientation can be induced by temperature or pressure (Sutrakar *et al.*, 2012). The study of the orientation effect on superlattices and/or quantum wells is a well documented topic and is still of actuality and importance (Kajikawa, 2012; Assa Aravindh *et al.*, 2012). The presence of built-in *permanent* piezoelectric fields in (111)- and (311)-oriented superlattices (SLs) and the progress in crystal growth processes have renewed the interest in these systems due to the potential they present for nanophononics which manipulates sound and heat at the nanoscale (acoustic phonons of gigahertz–terahertz frequencies and nanometer wavelengths; Reparaz *et al.*, 2010; Rozas *et al.*, 2005, 2008; Mintairov & Melehin, 1999; Lambert & Srivastava, 1999). The importance of these systems is also greatly due to the intrinsic limitations of the '*usual*' nanowave phononic devices represented by mirrors, cavities and monochromatic phonon sources, due to the weakness of their deformation potential which couples acoustic phonons to electrons.

Piezoelectric fields can be induced by strain in zinc blende phases and their (001)-oriented SLs, but these structures do not present spontaneous electric fields because of their high degree of symmetry. However, it has been observed that if the growth axis of the SL is different from (001), noncentrosymmetric crystals are obtained with large, permanent and spontaneous strain-induced piezoelectric fields (they can reach more than 10^5 V cm^{-1}; Smith, 1986; Mailhiot & Smith, 1987; Laurich *et al.*, 1989; Caridi *et al.*, 1990). Huge efficiencies for coherent acoustic phonon generation have been reported in GaInN/GaN SLs and a similar effect was reported in piezoelectric GaInAs/AlAs SLs (Reparaz *et al.*, 2010; Rozas *et al.*, 2008).

Earlier, it has been shown that these permanent built-in piezoelectric fields can also be used to produce a 2DEG (two-dimensional electron or hole gas) in order to replace the extrinsic doping (Snow *et al.*, 1990). Compared with the (001)-

SLs, the piezoeletrically active (111)-SLs were found to possess large and linear electro-optic coefficients (Mailhiot & Smith, 1988*a*) and a much more pronounced variation of their resistivity (Konczewicz *et al.*, 2001). These fields modify the optical properties of the SL and can lead to very strong nonlinearities (Mailhiot & Smith, 1988*b*; Smith & Mailhiot, 1987) which are useful for non-linear optical devices (Mailhiot & Smith, 1987). Growth directions other than (001) can also be used to obtain a high mobility carrier (Los *et al.*, 1995) and to modify the opto-electronic properties (Mireles & Ulloa, 2000). Epitaxial growth along the nonprincipal (001) crystallographic axis has allowed the fabrication of quantum well lasers of good quality (Batty *et al.*, 1989; Meney, 1992; Foreman, 1994; Hayakawa, Kondo *et al.*, 1988; Hayakawa, Suyama *et al.*, 1998*a*,*b*; Hayakawa, Takahashi, Kondo *et al.*, 1988*a*,*b*; Hayakawa, Takahashi, Suyama *et al.*, 1988). In the high-temperature regime, polar optical phonon scattering is found to contribute to the increase in thermoelectric power S as has been observed in (111)-oriented PbTe/PbEuTe multiple quantum-wells (Koga *et al.*, 1999). Different values of the magnetocrystalline anisotropy have been obtained in (001)-, (110)- and (111)-oriented Co-Pt SLs because of the epitaxy along different orientations which can induce defects and local lattice distorsions (Lee *et al.*, 1990).

To our knowledge the problem of SLs with various growth-axis directions has often been addressed by means of the envelope function approach (Kajikawa, 2012; Los *et al.*, 1995; Hayakawa, Kondo *et al.*, 1988; Hayakawa, Suyama *et al.*, 1998*a*,*b*; Hayakawa, Takahashi, Kondo *et al.*, 1988*a*,*b*; Hayakawa, Takahashi, Suyama *et al.*, 1988; Vina & Wang, 1986; El Khalifi *et al.*, 1990; Gil *et al.*, 1990) and rarely by other methods such as the tight-binding approach (Wang & Ting, 1995) or the first-principles methods (Assa Aravindh *et al.*, 2012; Rubio *et al.*, 1994; Picozzi *et al.*, 1997; Magri, 1990; Bungaro & Rabe, 2002; Tair *et al.*, 2007; Badi *et al.*, 2008). The first-principles methods are particularly needed to investigate *microscopically* these specific systems.

Our aim here is to investigate the symmetry of (111)-oriented SLs but also to give all the details concerning the (001) and (110) symmetries. These details are presented in such a way that they can be directly implemented in the LmtART code (Savrasov, 1996) which uses an accurate first-principles full-potential linear muffin-tin orbital (FPLMTO) band-structure method. Standard GaAs/AlAs SLs have been selected for the test since the latter are well known materials and do not present any complication for convergence. The paper is organized as follows: In §2 the crystallographic parameters of our SL crystals are calculated. In particular, the case of (111)-SLs has been emphasized while the (001)- and (110)-SLs have been summarized and all the details necessary for the lmtART implementation are given. In §3 the results of §2 are applied to GaAs/AlAs standard SLs. A general conclusion is then given in §4.

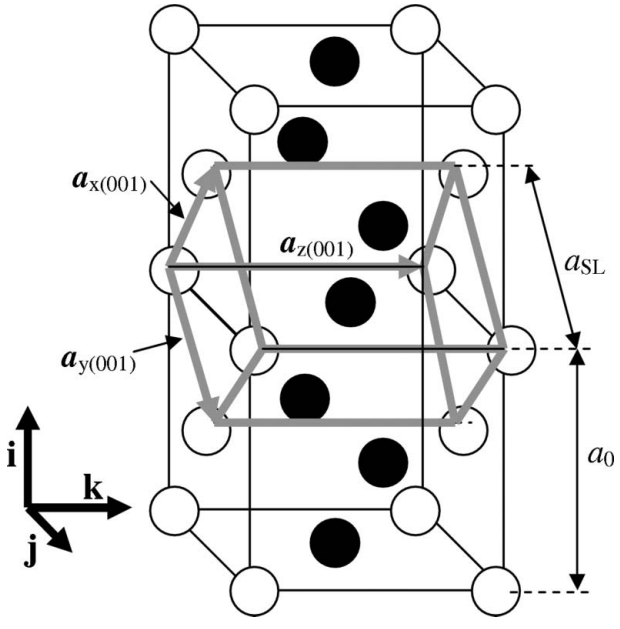

Figure 1
The direct zones of the bulk semiconductor and a (001)-growth axis SL(1,1). The set of primitive translation vectors $\boldsymbol{a}_{x(001)}$, $\boldsymbol{a}_{y(001)}$, and $\boldsymbol{a}_{z(001)}$ of the SL (1,1) are also shown. $\boldsymbol{i}$, $\boldsymbol{j}$ and $\boldsymbol{k}$ are the Cartesian unitary vectors. Every dot represents a node containing two atoms, one anion and one cation. a_0 and a_{SL} represent the lattice constants of the bulk and the superlattice respectively.

2. Crystallographic investigation

The investigated structures consist of ideal quantum well superlattices SL(m,n) made of a periodical sequence of m monolayers of GaAs atoms and n monolayers of AlAs atoms (a monolayer contains two atoms, one cation and one anion). For convenience, only cases for which $(m + n)$ is even are considered here. Bulk GaAs and AlAs have zinc-blende-like structures and their SL systems have different symmetries depending on their orientation (growth axis). Both (001)- and (110)-oriented SLs have a tetragonal symmetry but the case of (111)-oriented SLs is more complicated: both the (111)-SL direct and reciprocal primitive cells resemble greatly the case of face-centred cubic (f.c.c.) crystals with the little difference that the length of one primitive translation vector is different from the two other primitive vectors length; more details are given below. Some details and discussion on the symmetry of (001)- and (110)-oriented SLs can also be found in previous works (Gell *et al.*, 1987; Tair *et al.*, 2007; Badi *et al.*, 2008). Details concerned with the (111)-SLs are more difficult to find in the literature but are not totally absent (Magri, 1990; Bungaro & Rabe, 2002).

The primitive translation vectors (PTV) of the direct lattice of the bulk materials write: $\boldsymbol{a}_x = (1,0,1)a_0/2$; $\boldsymbol{a}_y = (1,1,0)a_0/2$; $\boldsymbol{a}_z = (0,1,1)a_0/2$, where a_0 represents the lattice parameter of the bulk. The PTV of their reciprocal lattice write: $\boldsymbol{g}_x = (1,-1,1)2\pi/a_0$; $\boldsymbol{g}_y = (1,1,-1)2\pi/a_0$; $\boldsymbol{g}_z = (-1,1,1)2\pi/a_0$. Any other vector of the reciprocal lattice of bulk writes as a linear combination of the latter: $\boldsymbol{G}_{bulk} = h\boldsymbol{g}_x + k\boldsymbol{g}_y + l\boldsymbol{g}_z = (2\pi/a_0)(h + k - l, -h + k + l, h - k + l)$, where h, k and l are positive or negative integers. The volume of the bulk direct primitive unit

Table 1
Coordinates of the atomic positions in successive planes of the (001)-SL.

Each successive line corresponds to a plane containing Ga (or Al) in the first one and As in the second line. The planes involved in (001)-SL(m,n) with $m + n = 2$ are the four first lines and those involved in the case of $m + n = 4$ are all the eight listed lines. We have used no simplification (for example, we have written $4/4L$ instead of $1/L$) in order to show to the reader how to easily infer the following lines.

		x	y	z		x'	y'	z'
$m+n=4$, *i.e.* $L=2$	$m+n=2$, *i.e.* $L=1$	0	0	0		0	0	0
		1/4	1/4	1/4		1/2	0	$1/4L$
		0	1/2	2/4		1/2	1/2	$2/4L$
		1/4	3/4	3/4	→	1	1/2	$3/4L$
		0	0	4/4		0	0	$4/4L$
		1/4	1/4	5/4		1/2	0	$5/4L$
		0	1/2	6/4		1/2	1/2	$6/4L$
		1/4	3/4	7/4		1	1/2	$7/4L$

cell is $V_{\rm bulk} = a_0^3/4$ and there are two atoms per unit cell, one Ga (or Al) and one As.

The PTV of the direct lattice of (001)-SL write: $\boldsymbol{a}_{x(001)} = (1,1,0)a_0/2$; $\boldsymbol{a}_{y(001)} = (-1,1,0)a_0/2$; $\boldsymbol{a}_{z(001)} = (0,0,L)a_0$, with $L = (m + n)/2$. The volume of the (001)-SL direct primitive unit cell is $V_{(001)} = La_0^3/2$ which means that $V_{(001)\rm SL} = 2LV_{\rm bulk}$, and there are $4L = 2(m + n)$ atoms per unit cell: m atoms of Ga, n atoms of Al, and $(m + n)$ atoms of As. In Fig. 1 we show the direct lattice of a (001)-growth axis SL(1,1) made up of an alternation of one monolayer of GaAs and another one of AlAs. The link between the bulk and the SL direct lattices is shown in the figure. The (001)-SL unit cell has a tetragonal symmetry with $a_{x(001)} = a_{y(001)} = a_{\rm SL} = a_0/\sqrt{2}$ and $a_{z(001)} = La_0$ so that in theory we have $a_{z(001)}/a_{x(001)} = L$ (In the first-principles structural calculations, we can also try to obtain this $a_{z(001)}/a_{x(001)}$ ratio by minimization).

The position of any atom which writes $\boldsymbol{R} = x\boldsymbol{i} + y\boldsymbol{j} + z\boldsymbol{k}$ in the orthonormal Cartesian set, ($\boldsymbol{i}$, $\boldsymbol{j}$ and $\boldsymbol{k}$ being its unitary vectors), writes in the (001)-SL PTV set as: $\boldsymbol{R} = x'\boldsymbol{a}_{x(001)} + y'.\boldsymbol{a}_{y(001)} + z'.\boldsymbol{a}_{z(001)}$. Thus

$$\boldsymbol{R} = (x' - y')/2\boldsymbol{i} + (x' + y')/2\boldsymbol{j} + Lz'\boldsymbol{k}. \quad (1)$$

The coordinates x', y' and z' of $\boldsymbol{R}$ in the (001)-SL PTV set can easily be inferred from its x, y and z coordinates in the orthonormal Cartesian set, we have $x = (x' - y')/2$, $y = (x' + y')/2$ and $z = Lz'$, so that $x' = x + y$, $y' = y - x$ and $z' = z/L$. An example of the atomic coordinates set which must be involved in the cases of $L = 1$ and $L = 2$ is listed in Table 1. For example, if we have a (001)-SL(1,1), the GaAs atomic positions in ($\boldsymbol{i}$,$\boldsymbol{j}$,$\boldsymbol{k}$) are (0,0,0) and (1/4,1/4,1/4) for Ga and As (first and second lines in Table 1), respectively, and those corresponding to AlAs are (0,1/2,2/4) and (1/4,3/4,3/4) for Al and As (third and fourth lines in Table 1). The corresponding coordinates in the (001)-SL PTV set are also shown in this table. In our calculations, we preferred to use x', y' and z' coordinates and the (001)-SL PTV set as an input. In doing so we have to consider $a_{x(001)}$ as the lattice constant and to set $a_{y(001)}/a_{x(001)} = 1$, $a_{z(001)}/a_{x(001)} = \sqrt{2}\,L$ [it is as if we have taken another orthonormal Cartesian set $\boldsymbol{a}_{x(001)}$, $\boldsymbol{a}_{y(001)}$ and $\boldsymbol{a}_{z(001)}$ with the third vector having a different length from the two others, we then selected the 'Cartesian system' option in the Mindlab visual environment of the lmtART code (Savrasov, 1996)].

The reciprocal lattice of the (001)-SL is represented in Fig. 2 for all values of m and n, $m + n$ being even [by anticipation, it has been presented in a unified manner in the case of the (110)-SL]. In the case of a (001)-SL(m,n), the high-symmetry points B and Y are always identical to R and X, respectively. This last remark also holds for the (110)-SL, but only in the particular case of $m = n = 1$.

Fig. 3 shows how the direct lattice of a (110)-growth axis SL(1,1) is constructed in the XY plane inside the bulk host

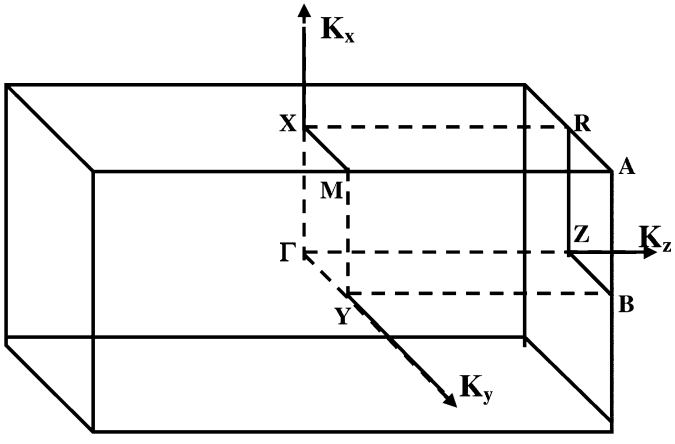

Figure 2
The Brillouin zone of both (001)- and (110)-growth axis SLs. The high-symmetry points B and Y are identical to R and X in the case of the (001) superlattices for any m and n ($m + n$ being even), and for the (110) SL(1,1) but they are different for all other cases.

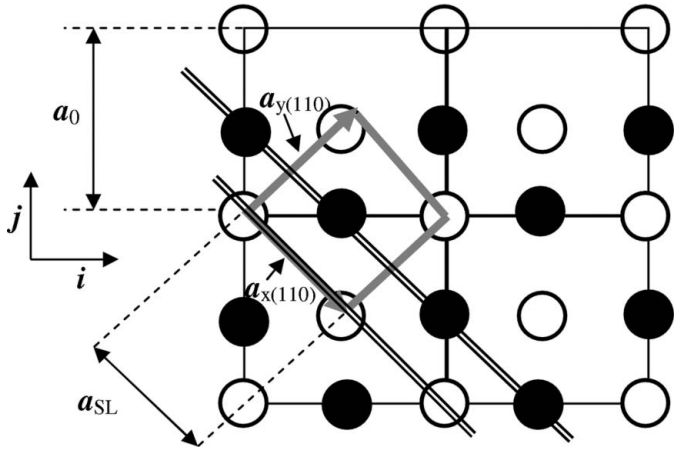

Figure 3
The X–Y contour plot of the direct zones of both bulk semiconductor and a (110)-growth axis SL(1,1). The set of primitive translation vectors $\boldsymbol{a}_{x(110)}$ and $\boldsymbol{a}_{y(110)}$ of the SL (1,1) are also shown in this figure. $\boldsymbol{i}$, $\boldsymbol{j}$ (and $\boldsymbol{k}$) are the Cartesian unitary vectors. The third primitive translation vector, $\boldsymbol{a}_{z(110)}$ (not represented), is equal to $\boldsymbol{k}$. Every dot represents a node containing two atoms, one anion and one cation. a_0 and $a_{\rm SL}$ represent the lattice constants of the bulk and the superlattice. In general $a_{y(110)} \neq a_{x(110)}$, except when $m = n = 1$ as in the present figure.

Table 2
Coordinates of the atomic positions in successive planes of the (110)-SL.

Each successive line corresponds to a plane containing Ga (or Al) in the first line and As in the second line. The planes involved in a (001)-SL(m,n) with $m + n = 2$ are the four first lines and those involved in the case of $m + n = 4$ are all the eight listed lines.

		x	y	z		x'	y'	z'
$m+n=4$, *i.e.* $L=2$	$m+n=2$, *i.e.* $L=1$	0	0	0		0	0	0
		1/4	1/4	1/4		0	1/2L	1/4
		1/2	0	1/2		1/2	1/2L	1/2
		3/4	1/4	3/4		1/2	2/2L	3/4
		1/2	1/2	0	→	0	2/2L	0
		3/4	3/4	1/4		0	3/2L	1/4
		1	1/2	1/2		1/2	3/2L	1/2
		5/4	3/4	3/4		1/2	4/2L	3/4

Table 3
Coordinates of the atomic positions in successive planes of the (111)-SL.

Each successive line corresponds to a plane containing Ga (or Al) in the first line and As in the second line. The first and second planes have to be involved in the case of a (111)-SL(m,n) with $m + n = 2$. If one deals with the case of $m + n = 4$, the four first planes have to be involved *etc.*

	(x, y, z)		(x^0, y^0, z^0)
First plane	(0, 0, 0)		(0, 0, 0)
	$\mathbf{T}$ = (1/4, 1/4, 1/4)		(0, 1/4L, 1/8)
Second plane	$\mathbf{R}$ = (1/2, 1/2, 0)		(0, 2/4L, 0)
	$\mathbf{R}$ + $\mathbf{T}$ = (3/4, 3/4, 1/4)		(0, 3/4L, 1/8)
Third plane	2$\mathbf{R}$ = (1, 1, 0)		(0, 4/4L, 0)
	2$\mathbf{R}$ + $\mathbf{T}$ = (5/4, 5/4, 1/4)		(0, 5/4L, 1/8)
Fourth plane	3$\mathbf{R}$ = (3/2, 3/2, 0)		(0, 6/4L, 0)
	3$\mathbf{R}$+$\mathbf{T}$ = (7/4, 7/4, 1/4)	→	(0, 7/4L, 1/8)
Fifth plane	4$\mathbf{R}$ = (2, 2, 0)		(0, 8/4L, 0)
	4$\mathbf{R}$ + $\mathbf{T}$ = (9/4, 9/4, 1/4)		(0, 9/4L, 1/8)
Sixth plane	5$\mathbf{R}$ = (5/2, 5/2, 0)		(0, 10/4L, 0)
	5$\mathbf{R}$ + $\mathbf{T}$ = (11/4, 11/4, 1/4)		(0, 11/4L, 1/8)
	–		–
nth plane	$(n-1)\mathbf{R}$ = ($(n-1)/2$, $(n-1)/2$, 0)		(0, $(2n-2)$/4L, 0)
	$(n-1)\mathbf{R}$ + $\mathbf{T}$ = ($(2n-1)/4$, $(2n-1)/4$, 1/4)		(0, $(2n-1)$/4L, 1/8)

materials. The direct lattice for a (110)-SL(1,1) is the same as that of the (001)-SL(1,1), the difference between these two kinds of SLs starts to appear from $m + n \geq 2$. The link between the bulk and the (110)-SL direct lattices is shown in the figure. The (110)-SL unit cell has a tetragonal symmetry with $a_{x(110)} = a_{\rm SL} = a_0/\sqrt{2}$, $a_{y(110)}/a_{x(110)} = L$ and $a_{z(110)}/a_{x(110)} = \sqrt{2}$. (In first-principle calculations, we can also try to obtain these two ratios by minimization.) As pointed out above, the reciprocal lattice of both (001)- and (110)-growth axis SL(m,n) can be represented in a unified manner for all values of m and n, $m + n$ being even (Fig. 2). We shall note that for the (110)-SL, the high-symmetry points B and Y are identical to R and X, respectively, when $m = n = 1$. However, B becomes different from R and Y from X for all other values of m and n ($m + n$ being even).

The PTV of the direct lattice of the (110)-SL write: $\boldsymbol{a}_{x(110)} = (1,-1,0)a_0/2$; $\boldsymbol{a}_{y(110)} = (L,L,0)a_0/2$; $\boldsymbol{a}_{z(110)} = (0,0,1)a_0$, with $L = (m + n)/2$. The volume of the (110)-SL direct primitive unit cell is also $V_{(110)} = La_0^3/2$, *i.e.* $V_{(110)\rm SL} = 2LV_{\rm bulk}$ like for the previous (001)-SL. Here also there are $4L = 2(m + n)$ atoms per unit cell: m atoms of Ga, n atoms of Al, and $(m + n)$ atoms of As. The coordinates x', y' and z' of the position R of any atom in the (110)-SL PTV set is linked to its x, y and z coordinates in the $\boldsymbol{i}$, $\boldsymbol{j}$, $\boldsymbol{k}$ orthonormal Cartesian set *via* the relations: $x' = x - y$, $y' = (x + y)/L$ and $z' = z$. An example of the atomic coordinates set which is involved in the cases of $L = 1$ and $L = 2$ is shown in Table 2. As for the previous (001) direction, here we preferred to use x', y' and z' coordinates and the (110)-SL PTV set as input, so $a_{x(110)}$ is set as the lattice constant, $a_{y(110)}/a_{x(110)} = L$ and $a_{z(110)}/a_{x(1101)} = \sqrt{2}$. We note that the high-symmetry points B and Y of the reciprocal lattice of the (110)-SL (Fig. 2) are identical to R and X only in the particular case of $m = n = 1$ and become different for all other values of m and n.

The case of (111)-oriented SLs is more complicated. For reasons of clarity, in Fig. 4(*a*) we separately show three successive monolayers (each one containing two atoms, Ga and As or Al and As); the $\boldsymbol{i}$, $\boldsymbol{j}$, $\boldsymbol{k}$ Cartesian unitary vectors are also shown. The unitary cell of the present (111)-SL is presented in Fig. 4(*b*) in which we remark on the non-orthonormal unitary basis set $\boldsymbol{i}'$, $\boldsymbol{j}'$, $\boldsymbol{k}'$. These two figures are grouped in Fig. 4(*c*) to show all the details. The relation between these two sets are: $\boldsymbol{i}' = (\boldsymbol{i} + \boldsymbol{k})/2$, $\boldsymbol{j}' = (\boldsymbol{j} + \boldsymbol{k})/2$ and $\boldsymbol{k}' = L(\boldsymbol{i} + \boldsymbol{j})$, with $L = (m + n)/2$, $m + n$ being even. $\boldsymbol{i}'$, $\boldsymbol{j}'$, $\boldsymbol{k}'$ are the PTV of the (111)-SL.

The present unitary cell with the non-orthonormal unitary basis set $\boldsymbol{i}'$, $\boldsymbol{j}'$, $\boldsymbol{k}'$ resembles a little that corresponding to the f.c.c. symmetry, the difference being that the third vector has a different length [it is $L.(\boldsymbol{i} + \boldsymbol{j})$ for (111) SL while it is $(\boldsymbol{i} + \boldsymbol{j})/2$ for f.c.c.]. Thus, the calculation of the first Brillouin zone will give us an octahedron like for f.c.c. with the difference that it will be 'compressed' in the third direction.

In order to perform first-principle calculations on (111)-SLs, we preferred to write the coordinates of $\boldsymbol{i}'$, $\boldsymbol{j}'$, $\boldsymbol{k}'$ which constitute the PTV of the (111)-SL using an orthogonal basis $\boldsymbol{i}^0$, $\boldsymbol{j}^0$, $\boldsymbol{k}^0$ of a tetragonal elementary cell (Fig. 5). The volume of the primitive cell is $V_{(111)\text{ primitive cell}} = \|(\boldsymbol{i}' \times \boldsymbol{j}')\boldsymbol{k}'\| = La_0^3/2$, and the volume of the present tetragonal non-primitive cell is $V_{(111)\text{ elementary cell}} = \|(\boldsymbol{i}^0 \times \boldsymbol{j}^0)\boldsymbol{k}^0\| = 4La_0^3$, it is easy to check that the multiplicity of the elementary cell is 8 (eight) by performing the calculation of the ratio ($V_{\text{elementary cell}}/V_{\text{primitive cell}}$). We also have $V_{(111)\text{ elementary cell}} = 16LV_{\rm bulk}$, $V_{(111)\text{ primitive cell}} = 2LV_{\rm bulk}$, and $4L = 2(m + n)$ atoms per unit cell [m for Ga, n for Al, and $(m + n)$ for As]. We have the following relations: $\boldsymbol{i}^0 = (\boldsymbol{i} - \boldsymbol{j})$, $\boldsymbol{j}^0 = L(\boldsymbol{i} + \boldsymbol{j})$ and $\boldsymbol{k}^{\boldsymbol{0}} = 2\boldsymbol{k}$, so that $\boldsymbol{i} = (\boldsymbol{i}^0 + \boldsymbol{j}^{\boldsymbol{0}}/L)/2$, $\boldsymbol{j} = (-\boldsymbol{i}^0 + \boldsymbol{j}^{\boldsymbol{0}}/L)/2$ and $\boldsymbol{k} = \boldsymbol{k}^0/2$. We can also find a relation between these vectors and the set vectors of the primitive cell: $\boldsymbol{i}' = (\boldsymbol{i}^0 + \boldsymbol{j}^0/L + \boldsymbol{k}^{\boldsymbol{0}})/4$, $\boldsymbol{j}' = (-\boldsymbol{i}^{\boldsymbol{0}} + \boldsymbol{j}^0/L + \boldsymbol{k}^0)/4$ and $\boldsymbol{k}' = \boldsymbol{j}^0$. Let us note that the lattice parameters of this tetragonal multiple cell are all different: $a_{x(111)} = a_{\rm SL} = \|\boldsymbol{i}^0\| = a_0\sqrt{2}$, $a_{y(111)} = \|\boldsymbol{j}^0\| = La_0\sqrt{2}$, and $a_{z(111)} = \|\boldsymbol{k}^0\| = 2a_0$. Thus, $a_{y(111)}/a_{x(111)} = L$ and $a_{z(111)}/a_{x(111)} = \sqrt{2}$ (also here one can try to obtain these ratios by minimization for first-principle calculations).

The coordinates x^0, y^0 and z^0 of the position $\boldsymbol{R}$ of any atom in the $\boldsymbol{i}^0, \boldsymbol{j}^0, \boldsymbol{k}^0$ set is linked to its x, y and z coordinates in the $\boldsymbol{i}$, $\boldsymbol{j}$, $\boldsymbol{k}$ orthonormal Cartesian set *via* the relations: $x^0 = (x - y)/2$, $y^0 = (x + y)/2L$ and $z^0 = z/2$. Hence, the atomic position writes: $\boldsymbol{R} = x\boldsymbol{i} + y\boldsymbol{j} + z\boldsymbol{k} = x^0\boldsymbol{i}^0 + y^0\boldsymbol{j}^0 + z^0\boldsymbol{k}^0$. So, knowledge of the atomic positions in the Cartesian basis allows us to infer their coordinates in the present $\boldsymbol{i}^0$, $\boldsymbol{j}^0$, $\boldsymbol{k}^0$ set. An example of the atomic coordinates set which is involved is shown in Table 3. This table dedicated to (111)-SLs is presented differently from the previous cases: the atomic positions, which have to be involved in the atomic basis, are given following the plane to which they belong (plane 1, plane 2 *etc.*). For example, if we have to calculate a (111)-oriented SL(1,1), we take the first plane for GaAs and the second plane for AlAs, and if we want to calculate a (111)-oriented SL(4,2), we take the first four planes for GaAs and the following two planes for AlAs *etc.*

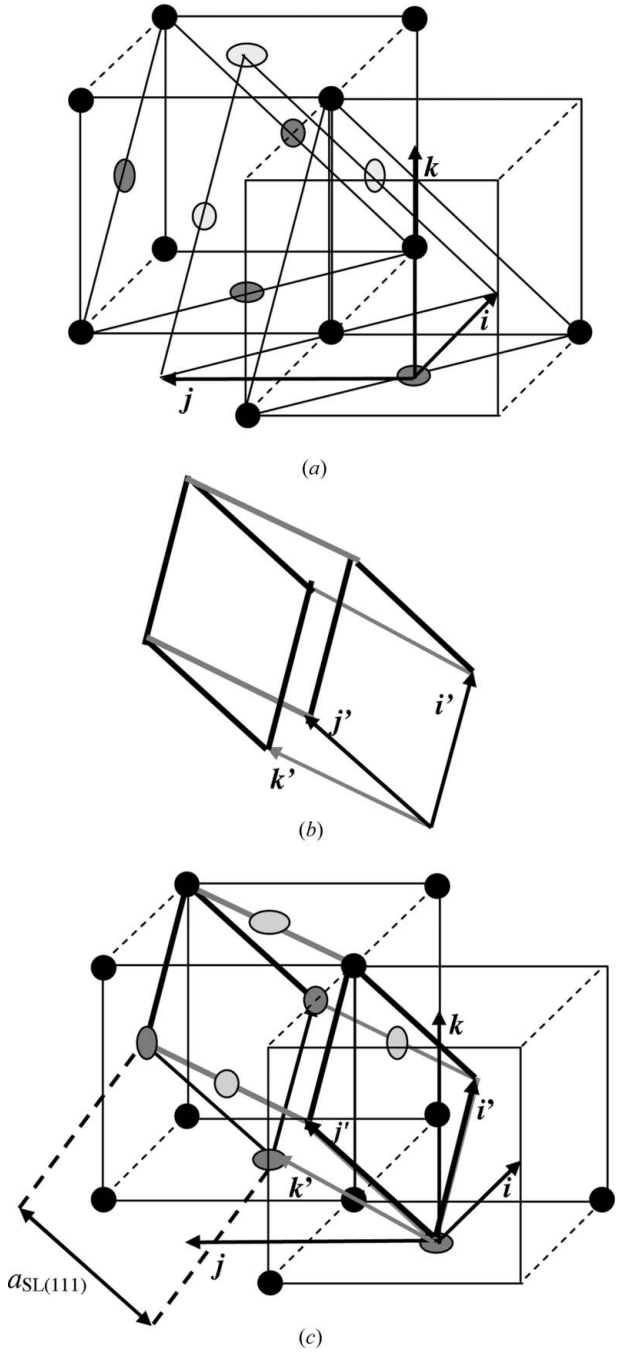

Figure 4
The construction of the primitive cell of a (111)-SL. $a_{SL(111)}$ represents the lattice constant of the superlattice. (*a*) Three successive monolayers (each one containing two atoms, Ga and As or Al and As); (*b*) the unitary cell of a (111)-SL(1,1) with a non-orthonormal unitary basis set $\boldsymbol{i}', \boldsymbol{j}', \boldsymbol{k}'$; (*c*) all the details of (*a*) and (*b*) grouped.

The set vectors $\boldsymbol{A}$, $\boldsymbol{B}$ and $\boldsymbol{C}$ of the primitive cell of the reciprocal lattice of (111)-oriented SL have been calculated

$$\boldsymbol{A} = 2\pi(\boldsymbol{j}' \times \boldsymbol{k}')/V_{\text{primitive cell}} = (2\pi/a_0)(-\boldsymbol{i} + \boldsymbol{j} - \boldsymbol{k}) \quad (2)$$

$$\boldsymbol{B} = 2\pi(\boldsymbol{k}' \times \boldsymbol{i}')/V_{\text{primitive cell}} = (2\pi/a_0)(\boldsymbol{i} - \boldsymbol{j} - \boldsymbol{k}) \quad (3)$$

$$\boldsymbol{C} = 2\pi(\boldsymbol{i}' \times \boldsymbol{j}')/V_{\text{primitive cell}} = (2\pi/a_0)(-\boldsymbol{i} - \boldsymbol{j} + \boldsymbol{k})/2L. \quad (4)$$

It is easy to remark from these relations that, as pointed out above, the primitive cell of the reciprocal lattice of (111)-SL is similar to the f.c.c. cell with the difference that the third vector is 'compressed' by a factor of $2L$. Hence, the high-symmetry points of (111)-SL will resemble those of f.c.c. in two directions and be different in the third by a constant factor. For example, in f.c.c. there are six equivalent X points, but in the present (111)-SL there are only four equivalent X points (denoted here as X_1 and X_2), while the two others denoted by X_3 will not be equivalent to them. This is how we obtained them in the Cartesian orthonormalized ($\boldsymbol{i}$, $\boldsymbol{j}$, $\boldsymbol{k}$) set (note that $a_{x(111)} = a_0\sqrt{2}$)

$$\boldsymbol{\Gamma} = (0, 0, 0) \quad (5)$$

$$\begin{aligned}\mathbf{M} \equiv \mathbf{L}_1 \equiv \boldsymbol{B} &= \frac{2\pi}{a_0}(\boldsymbol{i} - \boldsymbol{j} - \boldsymbol{k}) \\ &= \frac{2\pi}{a_{(111)\text{SL}}}\left(\sqrt{2}\boldsymbol{i} - \sqrt{2}\boldsymbol{j} - \sqrt{2}\boldsymbol{k}\right)\end{aligned} \quad (6)$$

$$\begin{aligned}\mathbf{M} \equiv \mathbf{L}_2 \equiv \boldsymbol{A} &= \frac{2\pi}{a_0}(-\boldsymbol{i} + \boldsymbol{j} - \boldsymbol{k}) \\ &= \frac{2\pi}{a_{(111)\text{SL}}}\left(-\sqrt{2}\boldsymbol{i} + \sqrt{2}\boldsymbol{j} - \sqrt{2}\boldsymbol{k}\right)\end{aligned} \quad (7)$$

$$\begin{aligned}\mathbf{L} \equiv \mathbf{L}_3 \equiv \boldsymbol{C} &= \frac{2\pi}{a_0}\frac{1}{2L}(-\boldsymbol{i} - \boldsymbol{j} + \boldsymbol{k}) \\ &= \frac{2\pi}{a_{(111)\text{SL}}}\left(-\frac{\sqrt{2}}{2L}\boldsymbol{i} - \frac{\sqrt{2}}{2L}\boldsymbol{j} + \frac{\sqrt{2}}{2L}\boldsymbol{k}\right)\end{aligned} \quad (8)$$

$$\begin{aligned}\mathbf{X} \equiv \mathbf{X}_1 \equiv \boldsymbol{B} + \boldsymbol{C} = \frac{2\pi}{a_{(111)\text{SL}}}\Bigg\{&\left(\sqrt{2} - \frac{\sqrt{2}}{2L}\right)\boldsymbol{i} \\ &- \left(\sqrt{2} + \frac{\sqrt{2}}{2L}\right)\boldsymbol{j} - \left(\sqrt{2} - \frac{\sqrt{2}}{2L}\right)\boldsymbol{k}\Bigg\}\end{aligned} \quad (9)$$

$$\mathbf{X} \equiv \mathbf{X}_2 \equiv \boldsymbol{A} + \boldsymbol{C} = \frac{2\pi}{a_{(111)\mathrm{SL}}}\left\{ -\left(\sqrt{2} + \frac{\sqrt{2}}{2L}\right)\boldsymbol{i} + \left(\sqrt{2} - \frac{\sqrt{2}}{2L}\right)\boldsymbol{j} - \left(\sqrt{2} - \frac{\sqrt{2}}{2L}\right)\boldsymbol{k}\right\} \quad (10)$$

$$\mathbf{Z} \equiv \mathbf{X}_3 \equiv \boldsymbol{A} + \boldsymbol{B} = \frac{2\pi}{a_0}(-2\boldsymbol{k}) = \frac{2\pi}{a_{(111)\mathrm{SL}}}\left(-2\sqrt{2}\boldsymbol{k}\right). \quad (11)$$

From these relations we see that $\mathbf{L}_1$ and $\mathbf{L}_2$ are equivalent; they will be denoted by the same **M** symbol, while the third point, denoted **L** (or $\mathbf{L}_3$), which is obtained directly from reciprocal lattice vectors, similar to the previous two points, has a different length. This also holds for the equivalent points $\mathbf{X}_1$ and $\mathbf{X}_2$, which will both be denoted by the symbol **X**, while the remaining point which is obtained by a similar combination of reciprocal lattice vectors has a different length and will be denoted as **Z** (or $\mathbf{X}_3$). These relations have to be rewritten in the $(\boldsymbol{i}^0, \boldsymbol{j}^0, \boldsymbol{k}^0)$ set because we have used it to write the PTV and the positions of the atoms constituting the basis. The following relations are obtained

$$\boldsymbol{\Gamma} = (0, 0, 0) \quad (12)$$

$$\mathbf{M} \equiv \mathbf{L}_1 \equiv \boldsymbol{B} = \frac{2\pi}{a_{(111)\mathrm{SL}}}\left(\sqrt{2}\boldsymbol{i}^0 - \sqrt{2}\boldsymbol{k}^0\right) \quad (13)$$

$$\mathbf{M} \equiv \mathbf{L}_2 \equiv \boldsymbol{A} = \frac{2\pi}{a_{(111)\mathrm{SL}}}\left(-\sqrt{2}\boldsymbol{i}^0 - \sqrt{2}\boldsymbol{k}^0\right) \quad (14)$$

$$\mathbf{L} \equiv \mathbf{L}_3 \equiv \boldsymbol{C} = \frac{2\pi}{a_{(111)\mathrm{SL}}}\left(-\frac{\sqrt{2}}{2L^2}\boldsymbol{j}^0 + \frac{\sqrt{2}}{2L}\boldsymbol{k}^0\right) \quad (15)$$

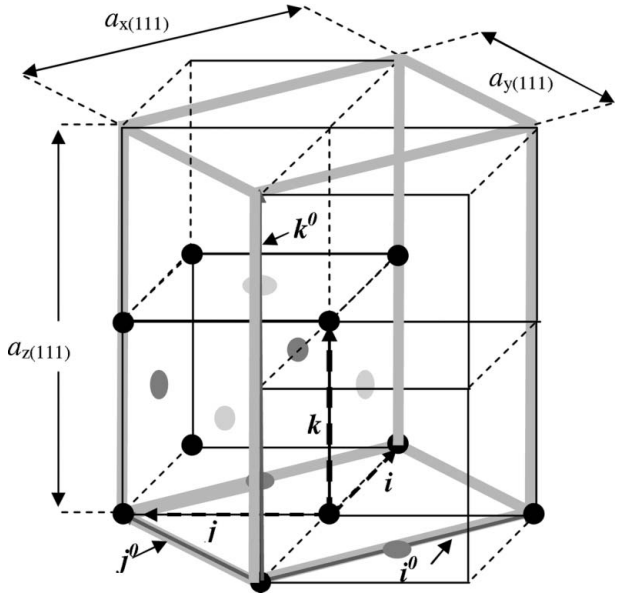

Figure 5
The non-primitive elementary tetragonal cell $(\boldsymbol{i}_0, \boldsymbol{j}_0, \boldsymbol{k}_0)$ selected for the study of (111)-oriented SLs.

$$\mathbf{X} \equiv \mathbf{X}_1 \equiv \boldsymbol{B} + \boldsymbol{C} = \frac{2\pi}{a_{(111)\mathrm{SL}}}\left\{\sqrt{2}\boldsymbol{i}^0 - \frac{\sqrt{2}}{2L^2}\boldsymbol{j}^0 + \left(-\sqrt{2} + \frac{\sqrt{2}}{2L}\right)\boldsymbol{k}^0\right\} \quad (16)$$

$$\mathbf{X} \equiv \mathbf{X}_2 \equiv \boldsymbol{A} + \boldsymbol{C} = \frac{2\pi}{a_{(111)\mathrm{SL}}}\left\{-\sqrt{2}\boldsymbol{i}^0 - \frac{\sqrt{2}}{2L^2}\boldsymbol{j}^0 + \left(-\sqrt{2} + \frac{\sqrt{2}}{2L}\right)\boldsymbol{k}^0\right\} \quad (17)$$

$$\mathbf{Z} \equiv \mathbf{X}_3 \equiv \boldsymbol{A} + \boldsymbol{B} = \frac{2\pi}{a_{(111)\mathrm{SL}}}\left(-2\sqrt{2}\boldsymbol{k}^0\right). \quad (18)$$

In our band structure calculations we will use the symbols **X**, **M**, **Γ**, **L** and **Z**. Fig. 6(*a*) shows the 'compressed' octahedron, which represents the first Brillouin zone of our (111)-oriented SL symmetry. For comparison we also show the well known octahedron which represents the first Brillouin zone of an f.c.c. (Fig. 6*b*).

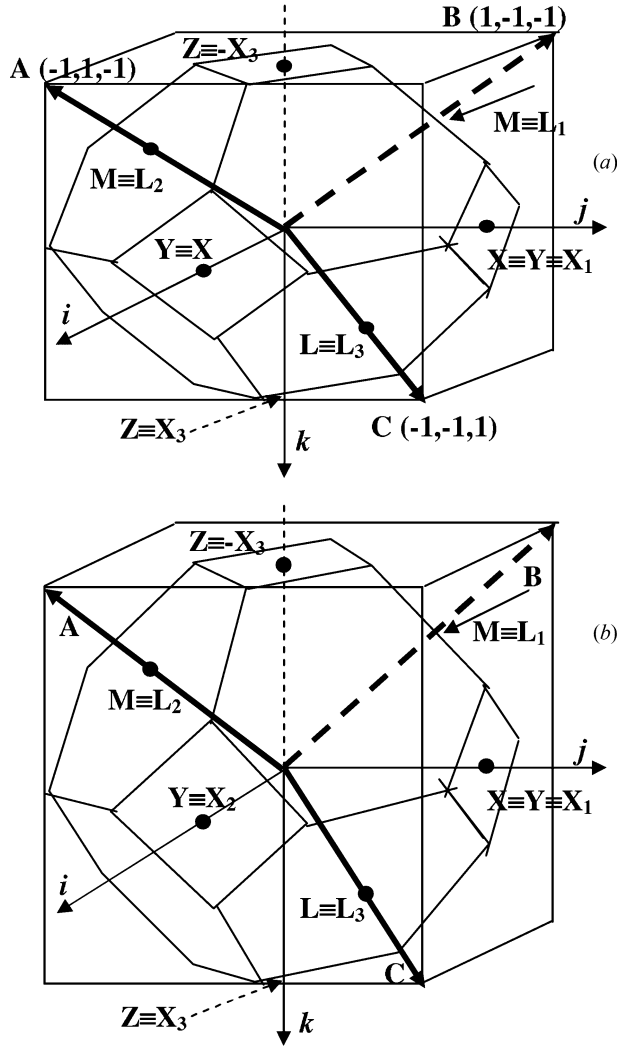

Figure 6
The first Brillouin zones (*a*) of our (111)-SL crystal which is represented by a 'compressed' octahedron, and (*b*) of a face-cubic centred (f.c.c.) crystal.

Table 4
The equilibrium lattice parameters for all cases (numerical values are in Å).

GaAs	AlAs	(001)-SL(1,1)	(110)-SL(1,1)	(111)-SL(1,1)
$a_0 = 5.649$	$a_0 = 5.655$	$a_0 = 5.652$	$a_0 = 5.652$	$a_0 = 5.652$
–	–	$a_{SL} = a_x = a_0/\sqrt{2}$	$a_{SL} = a_x = a_0/\sqrt{2}$	$a_{SL} = a_x = \sqrt{2}\, a_0$
–	–	$a_y = a_x$	$a_y = La_x$	$a_y = L\, a_x$
–	–	$a_z = \sqrt{2}La_x$	$a_z = \sqrt{2}a_x$	$a_z = \sqrt{2}\, a_x$

3. Application to band structure calculations

In this work we restrict ourselves to SLs with $m + n \leq 6$. Such systems can be considered as ultrathin SLs (USLs), which represent a special case to which several theoretical and also experimental efforts have been devoted in the past. This restriction is not only justified by the problem of time-demanding calculations, but also by the fact that such an investigation is sufficient for the present purpose. One very important point in this work is that the calculation test will be carried out on ideal cases in which all atoms (belonging to bulks or SLs) are located in ideal positions. The choice of short period USL systems makes this approximation acceptable, by which we assume the lattice parameter to be the same everywhere in the crystal since the distance between two consecutive interfaces is so small that a minimization calculation of the lattice constant may be enough. Thus, no relaxation calculation will be performed; this will save a significant time at low cost for precision.

We have utilized the local density approximation (LDA) based first principles FPLMTO method in its plane wave (PLW-FPLMTO) version, as implemented in the LmtART code (Savrasov, 1996). Compared with the FPLMTO version based on atomic sphere approximation (ASA-FPLMTO; Glötzel *et al.*, 1980; Christensen, 1988; Lambrecht & Segall, 1988), PLW-FPLMTO treats muffin-tin spheres (MTS) and interstitial regions on the same footing, leading to improvements in the precision of the eigenvalues. An unscreened long-range LMTO representation (Andersen, 1975) was used, and the radial wavefunctions have been adjusted to the spin average part of the potential in order to make them independent from the spin index. The crystal is

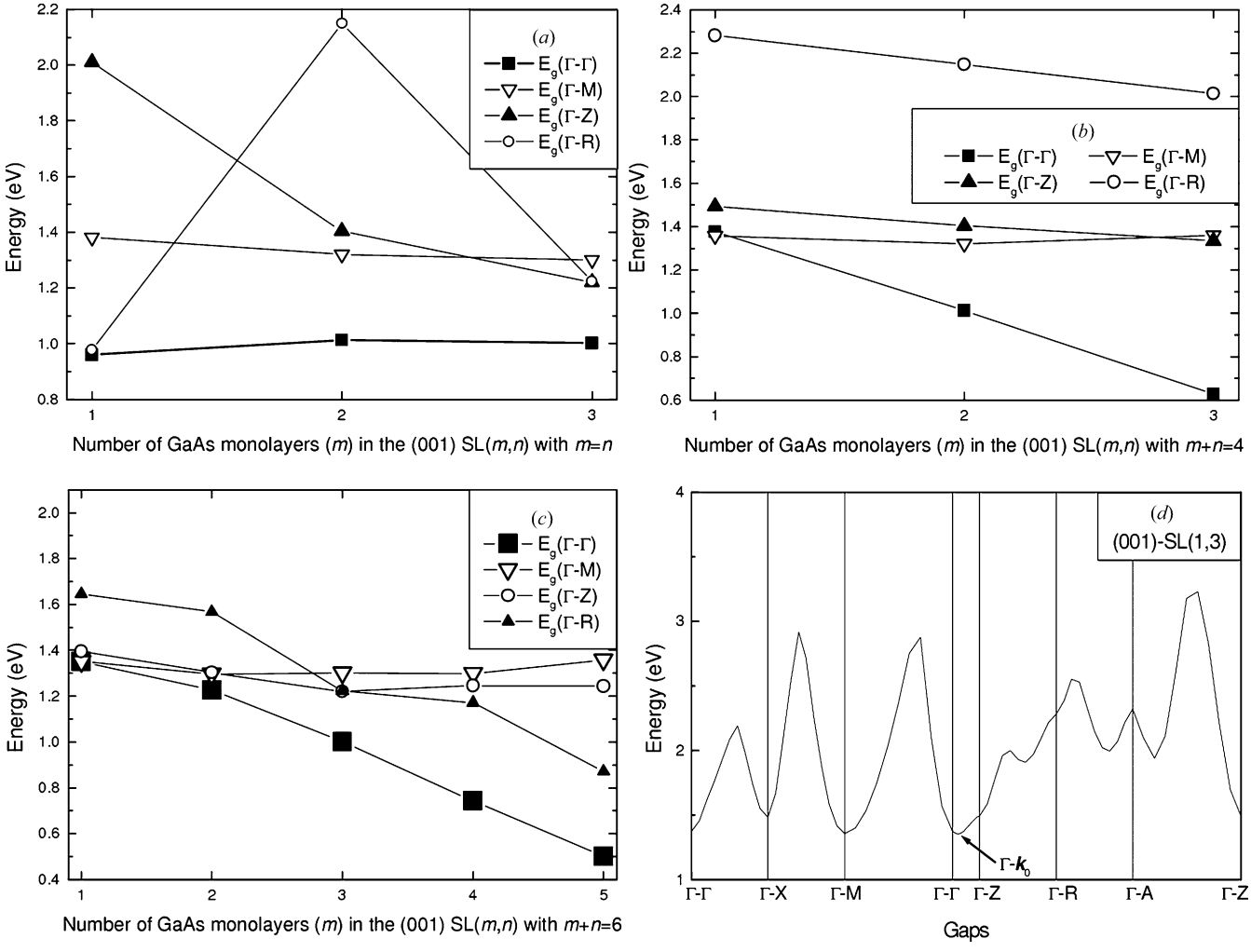

Figure 7
The gap variations for (001)-oriented SLs: (*a*) the case of $m = n$; (*b*) the case of $m + n = 4$; (*c*) the case of $m + n = 6$; (*d*) the case of SL(1,3), *i.e.* $m = 1$ and $n = 3$.

divided into two regions: non-overlapping muffin-tin spheres (MTS) surrounding every atom, and an interstitial region between these spheres. An MTS radius of 2.263 a.u. (atomic units) was used for both Ga and Al, and 2.355 a.u. was used for the As atom. These values were obtained by analyzing the crystal Hartree potential built with the help of the superposed atomic charge densities: this method is sufficient in the present case of AlGaAs systems. In the present PLW-FPLMTO calculation, the MTS have been taken to be non-touching for all atomic configurations, therefore, the minimum possible radii needs to be determined. Within the spheres, the non-overlapping MTS potential is expanded in spherical harmonics up to $l_{\max} = 6$ (in all cases), and in the interstitial regions it is Fourier transformed. The latter involves a number of plane waves which are determined automatically by the cut-off energies. The K-mesh is also set up differently following the case. The iteration process is repeated until the calculated total energy converges with a minimum accuracy of 10^{-7} Ry. The exchange correlation energy of electrons is described in the local density approximation (LDA) using the parameterization of Perdew & Wang (1992).

First, we calculated the equilibrium lattice parameters of bulk GaAs, bulk AlAs and the three kinds of SLs in the $m = n = 1$ case, *i.e.* (001)-, (110)- and (111)-oriented SL(1,1) systems. Using the minimization procedure the total energy was calculated for different values of the lattice constant, and the equilibrium corresponds to the lowest value of the total energy. Of course, the calculations for (001)- and (110)-SL(1,1) give the same result since their symmetry is the same for $m = n = 1$. Our calculations gave an equilibrium lattice constant for SL(1,1), which is approximately the average value of those of bulk GaAs and bulk AlAsa_0[SL(1, 1)] = (a_0[GaAs] + a_0[AlAs])/2, and since the lattice parameters of the two binaries are very close (minimization gives 10.68 and 10.69 a.u., *i.e.* 5.649 and 5.655 Å for GaAs and AlAs, respectively), a_0[SL(1, 1)] can be taken as to be equal to 10.685 a.u., *i.e.* 5.652 Å in all cases. The determination of the lattice parameters a_x, a_y and a_z for the three growth axis can be carried out using the formulae explained above and summarized in Table 4. Let us remark that instead of the great difference in symmetry between (110)- and (111)-SLs, their ratios a_y/a_x and a_z/a_x are similar. For (001)-, (110)- and (111)-

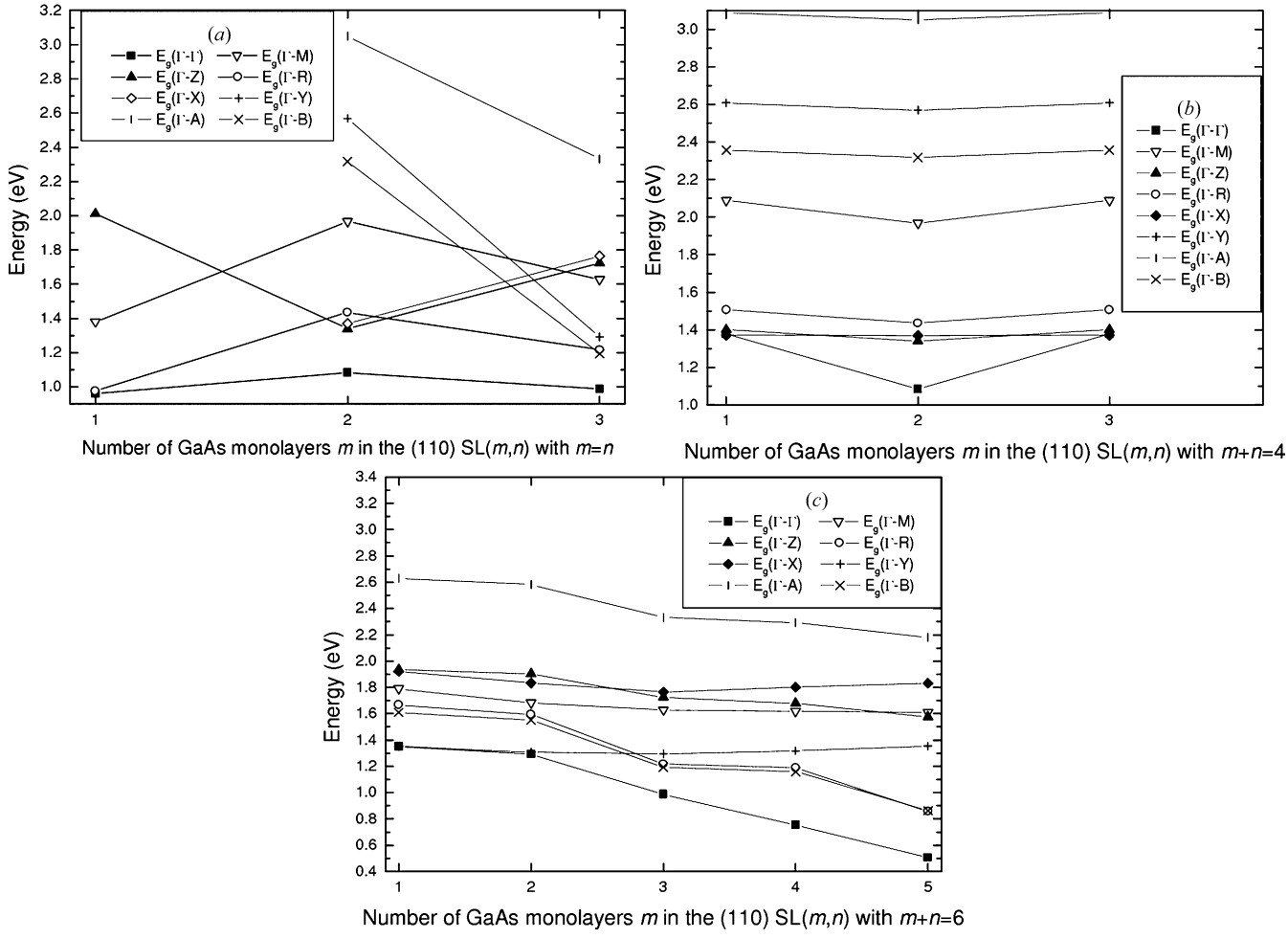

Figure 8
The gap variations for (110)-oriented SLs: (*a*) the case of $m = n$ for which some gaps have not been calculated when $m = 1$ because high-symmetry points *A*, *B* and *Y* do not exist; (*b*) the case of $m + n = 4$; (*c*) the case of $m + n = 6$. In (*a*) some gaps have not been presented for $m = n = 1$ because some high-symmetry points start to exist only after $m + n > 4$ in the case of the (110) direction (see above in the symmetry discussion).

SLs, the parameter $a_{SL} = a_x$ will be equal to ~ 3.99, ~ 3.99 and ~ 7.98 Å. It is clear that in the present case, the virtual crystal approximation (VCA) is valid and will be utilized for all other cases of SLs with other values of m and n. The following formula can be used to calculate a_0 but will not give a significant difference from the value of a_0 of SL(1,1): $a_0[\mathrm{SL}(m, n)] = (m.a_0[\mathrm{GaAs}] + n.a_0[\mathrm{AlAs}])/(m + n)$. Again, we want to underline that no minimization has been performed for the Y and Z directions and also relaxation has been ignored because we are dealing with thin SLs in which the distances between interfaces are too small (see text above).

It is well known that when aluminium is predominant in the AlGaAs ternary, and also when short-period GaAs–AlGaAs SLs are considered, these systems exhibit a type II configuration which is unsuitable for optical applications. For a reasonably long period and for small concentrations of Al these systems are type (I) SLs and are very good optical materials. In the present work we assume these facts and attract the attention of the reader to the fact that our purpose is not the investigation of the optical properties of these systems (which are in fact widely known), but to calculate the symmetry parameters and to perform a 'microscopic' test of the electronic properties of these systems for the different orientations. By 'microscopic' we mean at the atomic scale which is allowed by LDA-based first-principle methods.

Before calculating the band structures of (110)- and (111)-oriented SL systems, it is very important for a comparison to first revisit the case of the (001)-SLs. We see from Fig. 7(*a*) that for $m = n = 1$, the high symmetry point R is in competition with Γ, however, the Γ–R gap increases for higher values of m and n while the Γ–Γ fundamental gap remains approximately constant for all cases for which $m = n$. When $m \neq n$ (Figs. 7*b* and *c*), the Γ–Γ gap decreases rapidly with the number m of GaAs monolayers. We have checked that the reason for this behavior is that the (001) SL Γ–Γ gap follows the VCA; when $m = n$ this gap is the mean value of the gaps of the bulk materials so that it remains constant (Fig. 7*a*). However, when $m \neq n$ it is close to the Γ–Γ gap of the material which occupies the greater number of planes (Figs. 7*b* and *c*). This fact is not as obvious as it seems to be because the Γ–Γ gap of the SL is not only due to the Γ–Γ gaps of the bulks, but it takes its origin from the contribution of several other bulk gaps. It can easily be seen that this VCA behavior of the Γ–Γ gap is not obvious from the example of other gaps, such as Γ–R and Γ–Z for which the variation is clearly non-linear, the contribution of the bulk gaps being different from one case to another.

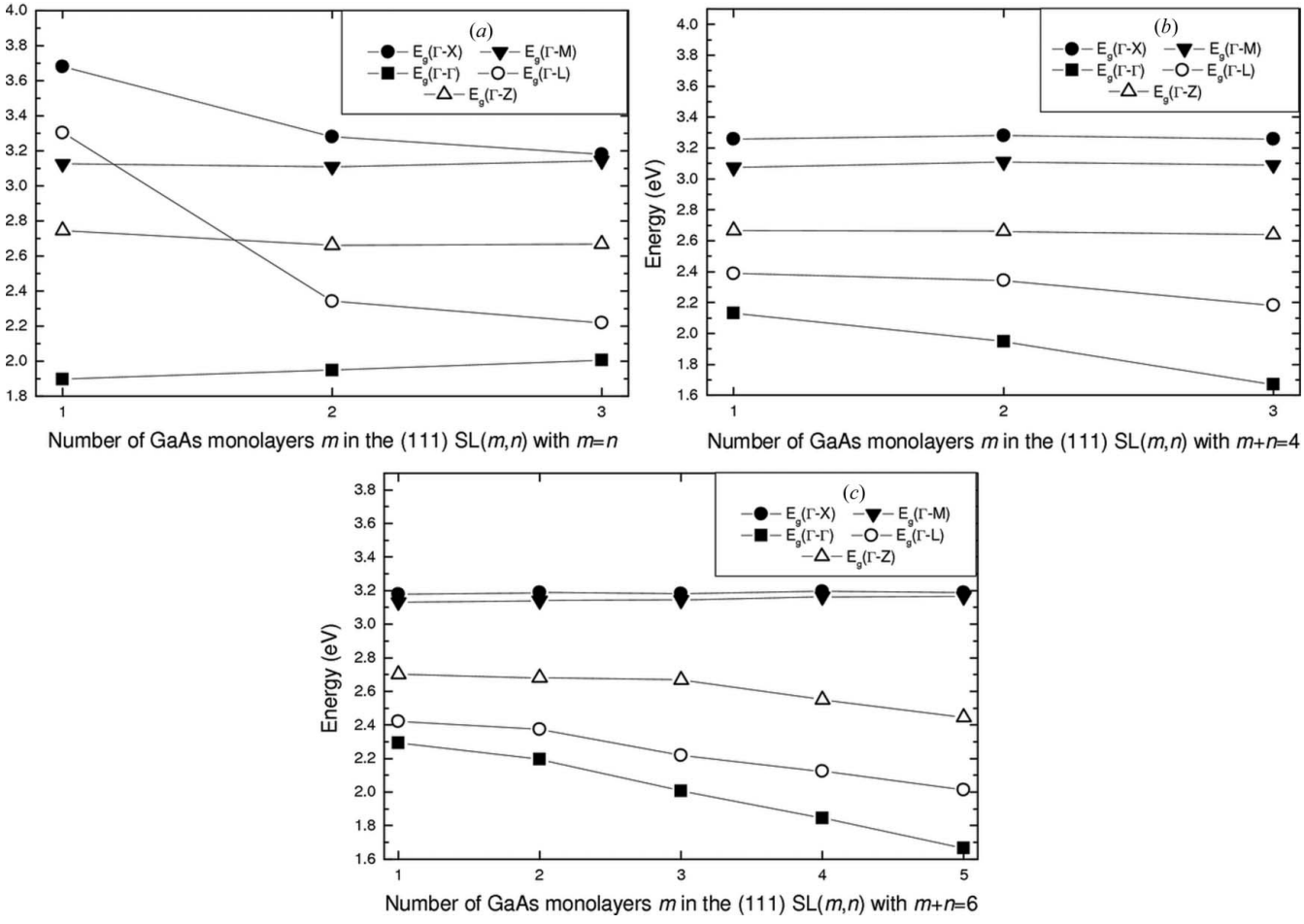

Figure 9
The gap variations for (111)-oriented SLs: (*a*) the case of $m = n$; (*b*) the case of $m + n = 4$; (*c*) the case of $m + n = 6$.

From Fig. 7 we see that the bottom of the conduction band (CB) is always located at Γ, except for SL(1,3) for which the bottom of the conduction band at M is lower. However, there is another wavevector $\boldsymbol{k}_0$ located between Γ and Z (Fig. 7*d*) at which the gap is lower, but the differences between Γ–M, $\boldsymbol{k}_0$–Γ and Γ—Γ are very small so the Γ–Γ gap can be considered as the fundamental gap in general. In most cases, the Γ–M and Γ–Z gaps are in competition.

From the fact that there is no competition with Γ for large m and n, one can understand one of the reasons for which the envelope function approximation (EFA) calculations is suitable for such systems. EFA is derived from a **K·P** effective mass Kane-like Hamiltonian and is therefore dedicated to the Brillouin zone center at Γ (Nag, 2002). The second fact that VCA works well (with the absence of significant bowing) for the present systems makes the conclusions of the present discussion independent from other parameters than the symmetry induced by the different growth axis.

In the case of SL(1,1) for which $m = n = 1$, *i.e.* both (001)- and (110)-SLs have identical direct and reciprocal lattices, they begin to be different for $m + n \geq 2$. The (110)-oriented SLs show some electronic similarities with the above (001)-SLs: for $m = n$ the Γ–Γ gap is almost constant (Fig. 8*a*), but for $m \neq n$ it decreases rapidly with the number m of GaAs monolayers (Figs. 8*b* and *c*). The competition between gaps shows some interesting features; high-symmetry points which are in competition with Γ–Γ are different following the value of m and n: In the case of SL(1,3), it is the Γ–X and Γ–Z gaps which are approximately equal to the Γ–Γ fundamental gap (Fig. 8*b*), but for $m \leq 2$ (so $n \leq 4$ when $m + n = 6$) it is the Γ–Y gap which is in competition with the Γ–Γ gap (Fig. 8*c*). Apart from the case of $m = n = 1$, no competition of Γ–Γ with Γ–R and Γ–M gaps has been observed. In this case also we note that VCA works well and that for increasing $m + n$ the Γ–Γ gap seems to be the fundamental gap without any competition. This second remark is not true in the case of $m = 3$ and $n = 1$, but this does not modify our conclusion because the latter is still in the limits of small values of $m + n$.

Contrary to the (110)-growth axis SLs, the (111)-oriented SLs are different from the (001)-SLs from the lowest values of m and n. The most important difference with the other orientations is that the Γ–Γ gap is always the fundamental one and that there is no competition with other gaps. However, the Γ–Γ gap variations look similar as for the previous orientations the latter is almost constant for $m = n$ (Fig. 9*a*) and decreases with m when $m \neq n$ (Figs. 9*b* and *c*). In Fig. 10 we have plotted the SL(3,3) band structures for the three orientations. The most important difference between the (001) and

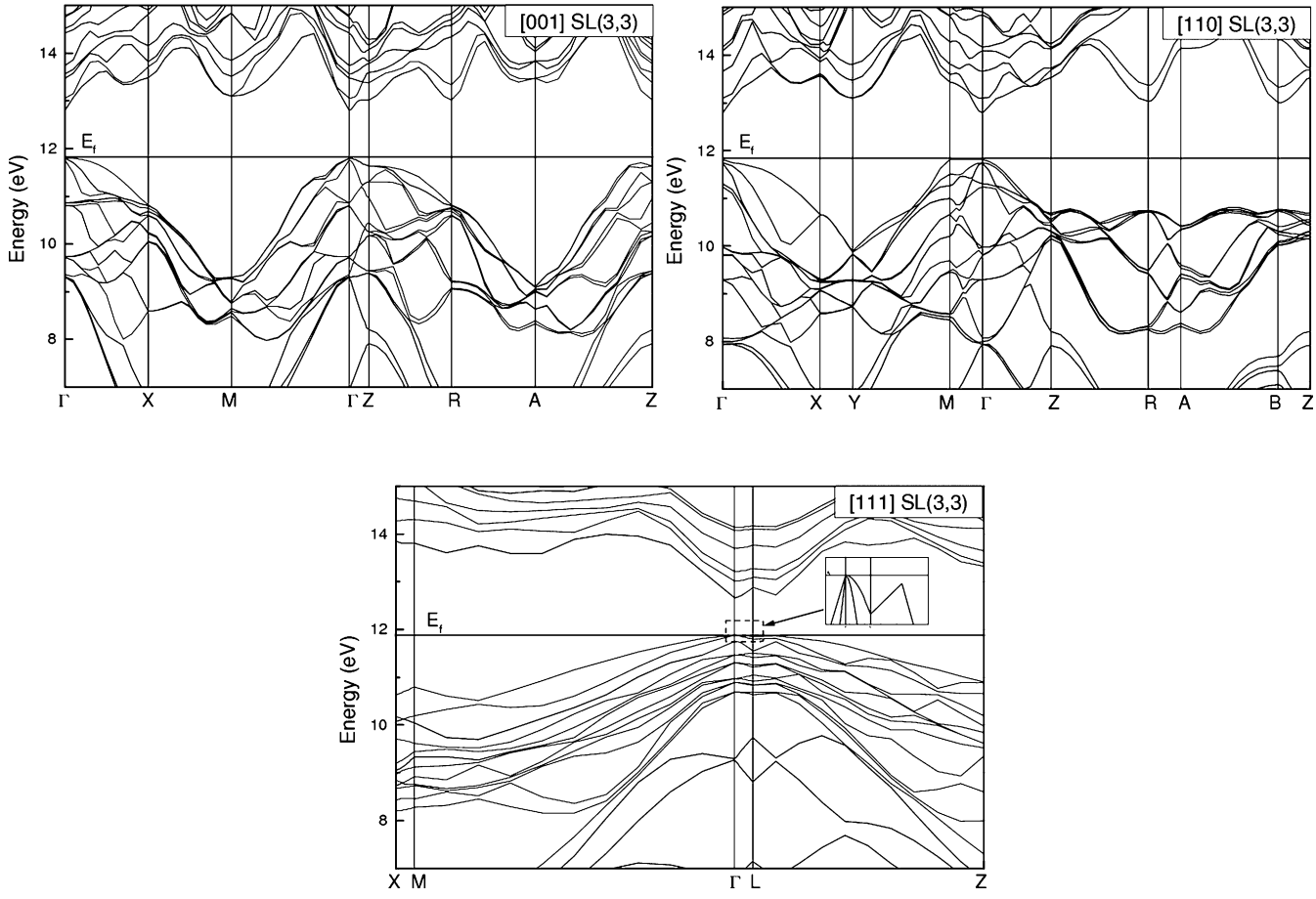

Figure 10
The band structures of SL(3,3) in three orientations.

(110) orientations is the flat valence band observed between Γ and *M* high-symmetry points in the (110) case, which means that for (110) the whole effective mass in this direction is significantly heavy. In the case of (111)-SL(3,3), it is clearly seen that the Γ–Γ gap is the fundamental gap and at the reverse of the other orientations all other gaps are higher than the Γ–Γ gap.

4. Conclusions

The symmetries of standard GaAs–AlAs superlattices oriented following the (001), (110) and (111) axes have been investigated and given in detail. The parameters obtained have been implemented and electronic properties of our systems have been calculated within the accurate 'plane wave' extension of the FPLMTO method. The data presented in the present paper may serve as a basis for further works dealing with the influence of the growth axis at the nanoscale.

One of us, NS, would like to thank Professor A. Benzair for valuable discussions. This work has been supported by the ENSET of Oran (Algeria), the Condensed Matter Section of Abdus Salam International Center for Theoretical Physics (ICTP, Trieste), by the Algerian National Research Projects CNEPRU under numbers (J3116/02/05/04, J3116/03/51/05, D05520060007, D05520080001, D05520100004) and by the Algerian National Project PNR entitled: 'Advanced Investigation of Nanostructures' (ADIN).

References

Andersen, O. K. (1975). *Phys. Rev. B*, **12**, 3060–3083.
Assa Aravindh, S., Jaya, S., Mathi, Valsakumar, M. C. & Sundar, C. S. (2012). *Superlattices Microstruct.* **51**, 92–102.
Badi, F., Louhibi, S., Aced, M. R., Mehnane, N. & Sekkal, N. (2008). *Physica E*, **41**, 45–49.
Batty, W., Ekenberg, U., Ghiti, A. & O'Reilly, E. P. (1989). *Semicond. Sci. Technol.* **4**, 904–909.
Bungaro, C. & Rabe, K. M. (2002). *Phys. Rev. B*, **65**, 224106.
Caridi, E. A., Chang, T. Y., Goossen, K. W. & Eastman, L. F. (1990). *Appl. Phys. Lett.* **56**, 659–661.
Christensen, N. E. (1988). *Phys. Rev. B*, **37**, 4528–4538.
El Khalifi, Y., Lefebvre, P., Allègre, J., Gil, B., Mathieu, H. & Fukunaga, T. (1990). *Solid State Commun.* **75**, 677–682.
Foreman, B. A. (1994). *Phys. Rev. B*, **49**, 1757–1766.
Gell, M. A., Ninno, D., Jaros, M., Wolford, D. J., Keuch, T. F. & Bradley, J. A. (1987). *Phys. Rev. B*, **35**, 1196–1222.
Gil, B., El Khalifi, Y., Mathieu, H., de Paris, C., Massies, J., Neu, G., Fukunaga, T. & Nakashima, H. (1990). *Phys. Rev. B*, **41**, 2885–2889.
Glötzel, D., Segall, B. & Andersen, O. K. (1980). *Solid State Commun.* **36**, 403–406.
Hayakawa, T., Kondo, M., Suyama, T., Takahashi, K., Yamamoto, S. & Hijikata, T. (1988). *Jpn. J. Appl. Phys.* **27**, L762–L765.
Hayakawa, T., Suyama, T., Takahashi, K., Kondo, M., Yamamoto, S. & Hijikata, T. (1988*a*). *J. Appl. Phys.* **64**, 297–302.
Hayakawa, T., Suyama, T., Takahashi, K., Kondo, M., Yamamoto, S. & Hijikata, T. (1988*b*). *Appl. Phys. Lett.* **52**, 339–341.
Hayakawa, T., Takahashi, K., Kondo, M., Suyama, T., Yamamoto, S. & Hijikata, T. (1988*a*). *Phys. Rev. B*, **38**, 1526–1528.
Hayakawa, T., Takahashi, K., Kondo, M., Suyama, T., Yamamoto, S. & Hijikata, T. (1988*b*). *Phys. Rev. Lett.* **60**, 349–352.
Hayakawa, T., Takahashi, K., Suyama, T., Kondo, M., Yamamoto, S. & Hijikata, T. (1988). *Jpn. J. Appl. Phys.* **27**, L300–L303.
Kajikawa, Y. (2012). *Superlattices Microstruct.* **51**, 16–52.
Koga, T., Harman, T. C., Cronin, S. B. & Dresselhaus, M. S. (1999). *Phys. Rev. B*, **60**, 14286–14293.
Konczewicz, L., Jouault, B., Contreras, S., Sadowski, M. L., Robert, J. L., Blanc, S. & Fontaine, Ch. (2001). *Phys. Status Solidi B*, **223**, 507–512.
Lambert, K. & Srivastava, G. P. (1999). *Physica B*, **263**, 517–521.
Lambrecht, W. R. & Segall, B. (1988). *Phys. Rev. Lett.* **61**, 1764–1767.
Laurich, B. K., Elcess, K., Fonstad, C. G., Beery, J. G., Mailhiot, C. & Smith, D. L. (1989). *Phys. Rev. Lett.* **62**, 649–652.
Lee, C. H., Farrow, R. F. C., Lin, C. J. & Marinero, E. E. (1990). *Phys. Rev. B*, **42**, 11384–11387.
Los, J., Fasolino, A. & Catellani, A. (1995). *Microelectron. J*, **26**, 745–749.
Magri, R. (1990). *Phys. Rev. B*, **41**, 6020–6031.
Mailhiot, C. & Smith, D. L. (1987). *Phys. Rev. B*, **35**, 1242–1259.
Mailhiot, C. & Smith, D. L. (1988*a*). *Phys. Rev. B*, **37**, 10415–10418.
Mailhiot, C. & Smith, D. L. (1988*b*). *Solid State Commun.* **66**, 859–863.
Meney, A. T. (1992). *Superlattices Microstruct.* **11**, 31–40.
Mintairov, A. M. & Melehin, V. G. (1999). *Semicond. Sci. Technol.* **11**, 904–911.
Mireles, F. & Ulloa, S. E. (2000). *Phys. Rev. B*, **62**, 2562–2572.
Nag, B. R. (2002). *Physics of Quantum Well Devices*. Dordrecht: Kluwer Academic Publishers.
Perdew, J. P. & Wang, Y. (1992). *Phys. Rev. B*, **45**, 13244–13249.
Picozzi, S., Continenza, A. & Freeman, A. J. (1997). *Phys. Rev. B*, **55**, 13080–13087.
Reparaz, J. S., Muniz, L. R., Goñi, A. R., Alonso, M. I., Rozas, G., Fainstein, A., Saravanan, S. & Vaccaro, P. O. (2010). *Phys. Rev. B*, **82**, 125306.
Rozas, G., Fainstein, A., Jusserand, B., Vaccaro, P. O. & Saravanan, S. (2008). *Phys. Rev. B*, **77**, 165314.
Rozas, G., Pascual Winter, M. F., Fainstein, A., Jusserand, B., Vaccaro, P. O., Saravanan, S. & Saito, N. (2005). *Phys. Rev. B*, **72**, 035331.
Rubio, A., Corkill, J. L. & Cohen, M. L. (1994). *Phys. Rev. B*, **49**, 1952–1956.
Savrasov, S. Y. (1996). *Phys. Rev. B*, **54**, 16470–16486, http://www.physics.ucdavis.edu/~mindlab/.
Smith, D. L. (1986). *Solid State Commun.* **57**, 919–921.
Smith, D. L. & Mailhiot, C. (1987). *Phys. Rev. Lett.* **58**, 1264–1267.
Snow, E. S., Shanabrook, B. V. & Gammon, D. (1990). *Appl. Phys. Lett.* **56**, 758–760.
Sutrakar, V. K., Mahapatra, D. R. & Pillai, A. C. (2012). *J. Phys. Condens. Matter*, **24**, 015401.
Tair, F., Sekkal, N., Amrani, B., Adli, W. & Boudaoud, L. (2007). *Superlattices Microstruct.* **41**, 44–55.
Vina, L. & Wang, W. I. (1986). *Appl. Phys. Lett.* **48**, 36–37.
Wang, E. G. & Ting, C. S. (1995). *Phys. Rev. B*, **51**, 9791–9800.